Please cite this article in press as: Gradinaru et al., Molecular and Cellular Approaches for Diversifying and Extending Optogenetics, Cell (2010), doi:10.1016/j.cell.2010.02.037

Resource

Cell

Molecular and Cellular Approaches for Diversifying and Extending Optogenetics

Viviana Gradinaru,[1,2,6] Feng Zhang,[1,5,6] Charu Ramakrishnan,[1] Joanna Mattis,[1,2] Rohit Prakash,[1,2] Ilka Diester,[1] Inbal Goshen,[1] Kimberly R. Thompson,[1] and Karl Deisseroth[1,3,4,*]
[1]Department of Bioengineering
[2]Program in Neuroscience
[3]Department of Psychiatry and Behavioral Sciences
[4]Howard Hughes Medical Institute
Stanford University, Stanford, CA 94305, USA
[5]Present address: Society of Fellows, Harvard University, Cambridge, MA 02138, USA
[6]These authors contributed equally to this work
*Correspondence: deissero@stanford.edu
DOI 10.1016/j.cell.2010.02.037

SUMMARY

Optogenetic technologies employ light to control biological processes within targeted cells in vivo with high temporal precision. Here, we show that application of molecular trafficking principles can expand the optogenetic repertoire along several long-sought dimensions. Subcellular and transcellular trafficking strategies now permit (1) optical regulation at the far-red/infrared border and extension of optogenetic control across the entire visible spectrum, (2) increased potency of optical inhibition without increased light power requirement (nanoampere-scale chloride-mediated photocurrents that maintain the light sensitivity and reversible, step-like kinetic stability of earlier tools), and (3) generalizable strategies for targeting cells based not only on genetic identity, but also on morphology and tissue topology, to allow versatile targeting when promoters are not known or in genetically intractable organisms. Together, these results illustrate use of cell-biological principles to enable expansion of the versatile fast optogenetic technologies suitable for intact-systems biology and behavior.

INTRODUCTION

A fundamental goal in biology is fast control of defined cells within functioning tissues. Temporal precision of control is important since cells may carry out fundamentally different computations and deliver different outputs depending on the timing and context of input signals. For example, it is almost meaningless to ask the causal role of "activation" or "inhibition" of a neuron type in the brain, since changes in context (Fleischmann et al., 2008) or millisecond-scale shifts in timing (Bi and Poo, 1998; Silberberg et al., 2004) can change the magnitude or flip the sign of neuronal action on the circuit. Similarly, pancreatic β cells execute synchronized oscillations in membrane potential resulting in pulsatile insulin secretion with precise timing across the population of β cells that may be important for the action of insulin on target tissues (Tengholm and Gylfe, 2009). Traditional genetics delivers cell type-specific control if adequate targeting strategies exist, but genetic approaches lack the temporal precision needed to control events with behaviorally or environmentally relevant triggering and timing; moreover, pharmacological control strategies lack cell type-specificity, temporal precision, or both. The general need to study molecular and cellular events not only in reduced systems, but also within intact biological systems, has driven recent awareness of the opportunities of fast control.

To enable temporally precise control of specific cell types within behaving animals, fast "optogenetic" (Deisseroth et al., 2006) technologies have been developed involving single-component light-responsive proteins that transduce brief pulses of light into well-defined action potential trains and effector functions in vivo (Boyden et al., 2005; Zhang et al., 2007a, 2007b). Through the use of optogenetics, precisely timed gain-of-function or loss-of-function of specified events can be achieved in targeted cells of freely moving mammals and other animals (Adamantidis et al., 2007). For example, we have found that direct light-triggered excitation of cellular electrical activity (depolarization and precisely timed action potentials) can be achieved via expression of the microbial opsin genes encoding *Chlamydomonas* channelrhodopsin-2 (ChR2) (Boyden et al., 2005) or *Volvox* channelrhodopsin-1 (VChR1) (Zhang et al., 2008). On the other hand, direct light-triggered inhibition of electrical activity (precisely timed hyperpolarization) can be achieved via expression of the *Natronomonas* halorhodopsin (NpHR) in vivo (Zhang et al., 2007a; Han and Boyden, 2007; Gradinaru et al., 2008); this halorhodopsin was selected for its step-like and highly stable photocurrents compared with other microbial generators of inhibitory current (Zhang et al., 2007a). The

Please cite this article in press as: Gradinaru et al., Molecular and Cellular Approaches for Diversifying and Extending Optogenetics, Cell (2010), doi:10.1016/j.cell.2010.02.037

halorhodopsin achieves inhibition by pumping into neurons an ion (chloride) that constitutes part of the natural mechanism of neuronal inhibition, and neurons are therefore well designed to process chloride influx (Zhang et al., 2007a); microbial proton pumps additionally can be used to achieve outward currents (Chow et al., 2010). Finally, more subtle (but still temporally precise) optical modulatory strategies are also possible, including changes in the input-output relationships of targeted cells via expression of engineered step function opsins, or "SFOs," that alter excitability (Berndt et al., 2009), and fast selective control of modulatory G_s or G_q signaling using synthetic rhodopsin/G protein-coupled receptor chimeras (optoXRs) (Airan et al., 2009). This collection of tools, along with the development of versatile devices to deliver light in vivo (Aravanis et al., 2007; Adamantidis et al., 2007; Gradinaru et al., 2007), has enabled widespread application of optogenetics.

To further expand the optogenetic toolbox, we have previously carried out genomic screening strategies to successfully identify and validate novel classes of opsins for optogenetic control (Zhang et al., 2007a, 2008) and carried out rationally designed mutagenesis to achieve new classes of opsin functionality (Berndt et al., 2009; Gunaydin et al., 2010). Here, we apply a third type of intervention, namely application of molecular trafficking strategies, to derive a panel of tools that both quantitatively and qualitatively enhance the power of optogenetics and open distinct avenues of investigation. In particular, tools are developed that allow targeting of cells solely by virtue of their topological relationships within tissue and that extend the reach of optical control to the infrared border, with effector function enhanced beyond the other known tools and covering the entire visible spectrum.

RESULTS

Membrane Trafficking and Microbial Opsin Genes

Deriving optogenetic tools from multiple classes of microbes promises substantial diversity of triggering and effector functions (Zhang et al., 2008), given the ecological diversity of microbial organisms occupying niches with a broad array of environmental signals of informational or energetic value (Yooseph et al., 2007). Moreover, as a necessary adaptation to small cell volume and genome size, microbes carry out sensation, transduction, and action via highly compact mechanisms, often all encompassed within a single open genetic reading frame (as with the microbial opsins, in which both photon sensation and ion flux effector function are implemented within a single compact protein) (Kalaidzidis et al., 1998; Lanyi and Oesterhelt, 1982; Lozier et al., 1975; Nagel et al., 2003). In contrast, metazoan or vertebrate cells may transduce energy or information with more complex multicomponent signaling cascades that afford greater opportunities for modulation but are much less portable (as with the vertebrate opsins). Optogenetic tools from simpler organisms therefore present clear opportunities, but may not express or be tolerated well by more complex cells. Indeed, archaeal halorhodopsin (the light-activated electrogenic chloride pump that can be used for optogenetic inhibition in metazoans) displays impaired subcellular localization when expressed at high levels in mammalian neurons (Gradinaru et al., 2008; Zhao et al., 2008). An early trafficking step, export from the endoplasmic reticulum (ER), was found to be impaired for this first-generation NpHR, leading to intracellular accumulations that colocalized with the ER marker KDEL (Figure 1A; Figure 1B, left). Fusion of the FCYENEV ER export motif from a vertebrate inward rectifier potassium channel to the NpHR C terminus prevented aggregate formation (Figure 1B, center) and greatly enhanced tolerability at high expression levels.

This second-generation enhanced tool (eNpHR, now eNpHR2.0) has been successfully employed in vivo and in intact tissue in a number of studies (Gradinaru et al., 2009; Sohal et al., 2009; Tønnesen et al., 2009; Arrenberg et al., 2009); expression was well tolerated, and additionally Thy1::eNpHR2.0 mice have been generated with well-tolerated long-term expression of eNpHR2.0 at high functional levels throughout the brain (G. Feng, G. Augustine, and K.D., unpublished data). As with many kinds of native inhibition, optogenetic inhibition could be overcome by strong excitatory activity (Sohal et al., 2009). Potential additional molecular modifications for enhancing photocurrents from known and emerging opsin gene family members would include signal peptides, additional ER export motifs, Golgi trafficking signals, transport signals, and other motifs involved in transport of membrane proteins along the secretory pathway to the cell surface (Simon and Blobel, 1993). We therefore sought to apply combinatorial membrane trafficking strategies that could be generally applicable in a systematic, principled fashion to candidate microbial membrane proteins for translation to metazoan applications.

Examination of eNpHR2.0-expressing hippocampal neurons revealed the absence of globular ER accumulations, as previously reported, but nevertheless persistent intracellular labeling and poor membrane localization (Figure 1B, center), suggesting that additional modifications subsequent to the ER export step would indeed be important. Examination of primary-sequence differences between two forms of an inward rectifier potassium channel with differential membrane localization (Kir2.1 and Kir2.4) revealed differences not only in C-terminal ER export motifs but also in N-terminal Golgi export signals and in C-terminal trafficking signals (Hofherr et al., 2005). Surprisingly, we found that provision of the Golgi export signal did not significantly affect surface expression (data not shown), but that addition of the trafficking signal from Kir2.1 either between eNpHR and the EYFP fusion, or at the C terminus of the fusion protein, dramatically reduced intracellular labeling and increased apparent surface membrane expression (Figure 1B, right) and also improved labeling of cellular processes (Figure 1B, right). Indeed, high-resolution confocal imaging (Figure 1C) revealed marked localization in processes, with identifiable labeled membranes spanning intracellular regions apparently devoid of the opsin-EYFP fusion protein, in a pattern never previously observed with NpHR or its derivatives.

If improved membrane targeting were indeed achieved with this modification, increased photocurrents would be anticipated to result. We therefore examined photocurrents, using whole-cell patch clamp recordings to quantify bona fide functional plasma membrane localization of halorhodopsin pump molecules. Photocurrents were indeed profoundly increased (to a level ~20-fold larger than the initially described NpHR currents;

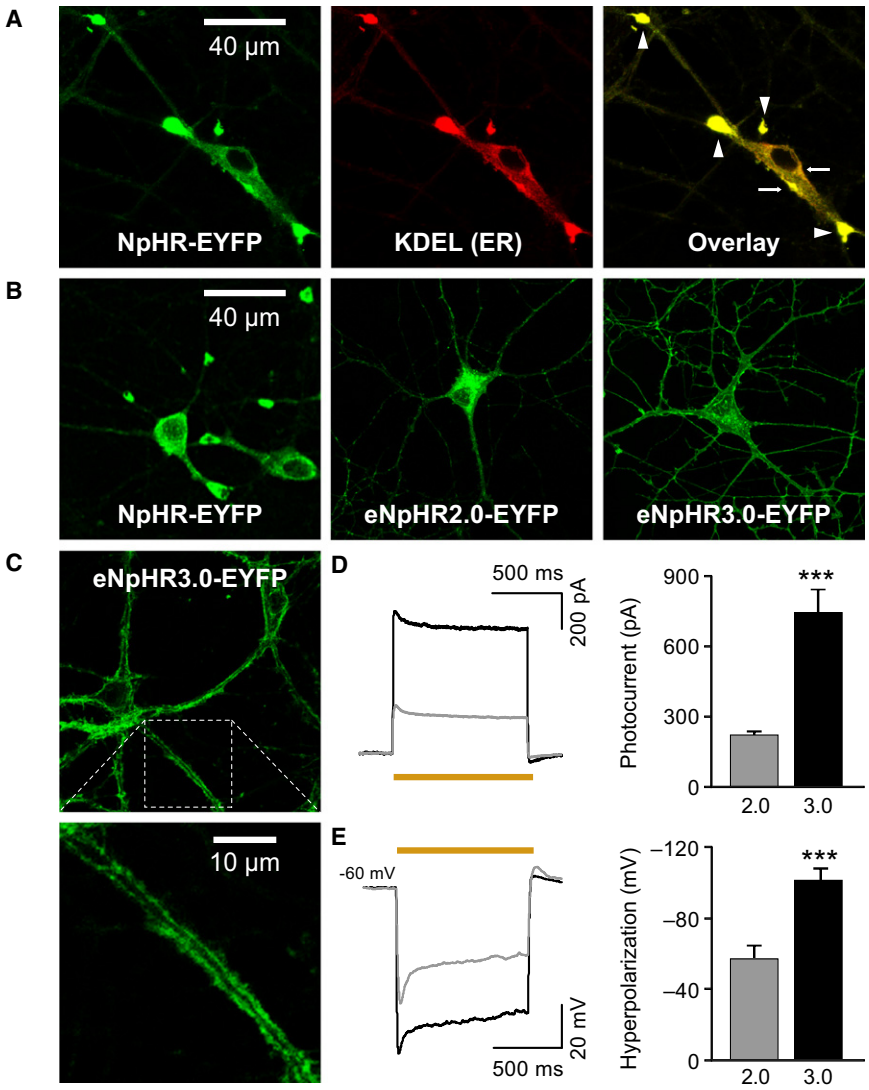

Figure 1. Multiple Trafficking Modules for Microbial Opsin Function in Mammalian Neurons

(A) Hippocampal neurons showing wild-type NpHR-EYFP aggregation in the ER. NpHR (green) and ER (red; immunostaining of the KDEL marker) are also shown in overlay (yellow) to illustrate colocalization of NpHR aggregates and ER (arrows, ER; arrowheads, ER aggregates).

(B) Multistep modification of wild-type NpHR (left) rescues membrane expression. Addition of the K-channel ER export motif (eNpHR2.0, middle) and trafficking signal (eNpHR3.0, right) respectively reduced ER aggregation and improved membrane expression (particularly in neuronal processes for 3.0).

(C) Membrane expression enabled in processes for eNpHR3.0 (confocal images showing membrane-localized EYFP fluorescence in the soma [top] and dendrite [inset, bottom]).

(D) Representative traces (left) showing photocurrents in cells virally transduced with eNpHR3.0 (black) and eNpHR2.0 (gray). Summary plot (right) showing average photocurrent levels in cells expressing eNpHR3.0 (747.2 ± 93.9 pA) and eNpHR2.0 (214.1 ± 24.7 pA; unpaired t test $p < 0.0005$; $n = 10$). Values plotted are mean ± SEM. Membrane input resistance was similar for all neurons patched (eNpHR2.0: 193.1 ± 36.6 MΩ; eNpHR3.0: 151.6 ± 28.5 MΩ; unpaired t test $p = 0.37$). Light delivery (593 nm) is indicated by the yellow bar.

(E) Representative traces (left) showing voltage traces in cells virally transduced with eNpHR3.0 (black) and eNpHR2.0 (gray). Summary plot (right) showing average hyperpolarization levels in cells expressing eNpHR3.0 (101.0 ± 24.7 mV) and eNpHR2.0 (57.2 ± 6.8 mV; unpaired t test $p < 0.0005$; $n = 10$).

See also Figure S1.

mean ± standard error of the mean [SEM], photocurrent 747.2 ± 93.9 pA in lentivirally transduced hippocampal pyramidal neurons under the human synapsin I promoter; n = 10; Figure 1D). At action spectrum peak described below, nanoampere-scale mean outward currents were readily observed with 3.5 mW/mm^2 yellow light, an order of magnitude lower intensity than required by proton pumps to attain this level of photocurrent (maintaining low light intensities becomes an important issue only for in vivo experiments, wherein safe control of significant tissue volumes is paramount) (Aravanis et al., 2007; Adamantidis et al., 2007; Chow et al., 2010). In virally transduced neurons, light-induced hyperpolarizations by >100 mV were routinely achievable, at the same modest light power levels (mean hyperpolarization 101.0 ± 24.7 mV; n = 10; Figure 1E). Membrane potential changes of this new magnitude represent a functionally distinct advance in optogenetic inhibition, and we accordingly designate this third-generation NpHR as eNpHR3.0 (the *Natronomonas* halorhodopsin was named NpHR in 2005 [Sato et al., 2005], and the first trafficking-enhanced version developed by Gradinaru et al. [2008] is now referred to as eNpHR2.0). As expected from prior work (Zhang et al., 2007a) showing that NpHR photocurrents were step-like and exhibited little inactivation over more than 10 min of continuous illumination (indeed, NpHR was selected for this reason, as described in Zhang et al. [2007a]), the eNpHR3.0 photocurrents were also step-like, resistant to inactivation, and highly stable over multiple light pulses and long (behaviorally relevant) timescales (Figure 1D; Figure S1 available online) (Zhang et al., 2007a).

Targeting by Connection Topology Enabled by Transcellular Trafficking

We asked whether the robust improved expression were preserved in the mammalian brain in vivo. We injected lentiviral vectors delivering the novel opsin gene under control of the CaMKIIα promoter to the CA1 region of the hippocampal formation in adult mice and examined distribution of the expressed EYFP fusion. As in cultured cells, strong expression was observed not only in dendrites but also in axons in vivo with

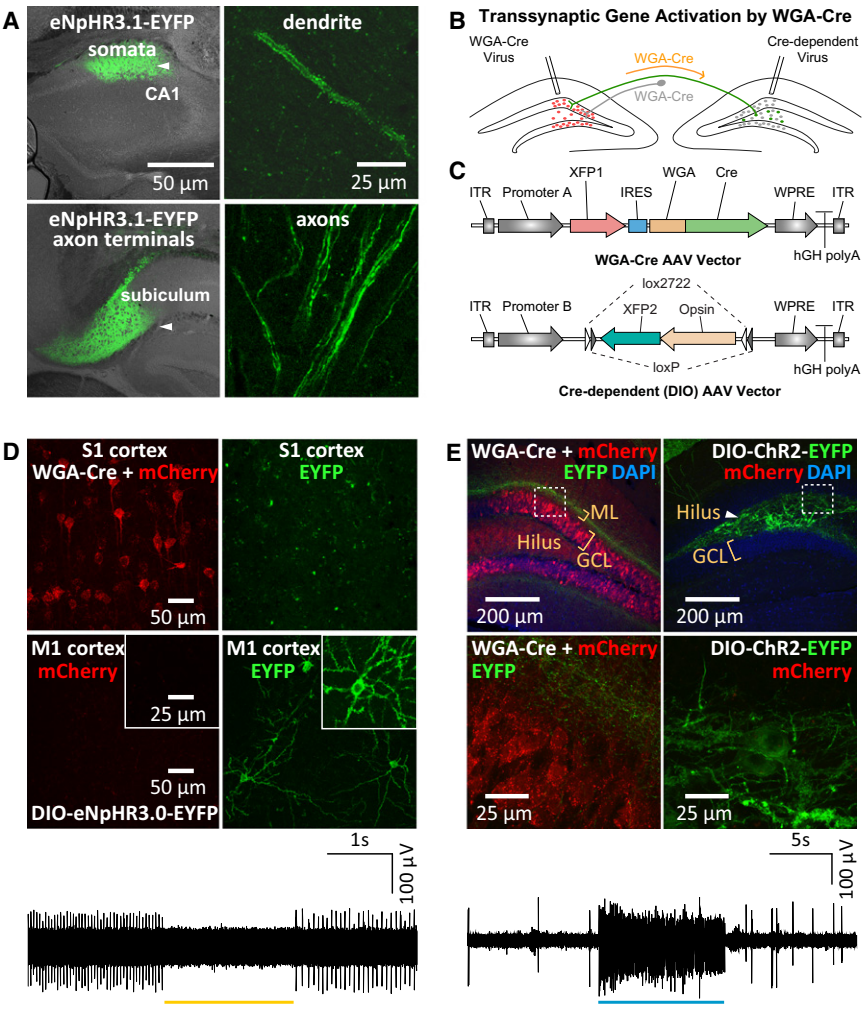

Figure 2. Trafficking-Enhanced Projection Targeting and Topological Targeting In Vivo

(A) Lentiviral delivery of eNpHR3.1 (shorter version of eNpHR3.0 with the N-terminal signal peptide removed; Experimental Procedures) driven by the CaMKIIα promoter led to expression in CA1 pyramidal neurons and dendrites (top; arrowhead indicates CA1), as well as in axon terminals (bottom; arrowhead indicates subiculum).

(B) Transcellular gene activation by wheat germ agglutinin (WGA)-Cre fusion. The schematic depicts two injection sites (one with WGA-Cre fusion gene and another with Cre-dependent opsin virus) and long-range projections; Cre can be transcellularly delivered from transduced cells (red) to activate distant gene expression only in connected neurons that have received the Cre-dependent virus (green), not in others (gray).

(C) Construct design for the WGA-Cre (top) and Cre-dependent (bottom) AAV vectors. WGA and Cre genes are both optimized with mammalian codons.

(D) Injection of AAV carrying the EF1α::mCherry-IRES-WGA-Cre cassette in the rat primary somatosensory cortex (S1) led to mCherry fluorescence in neuronal somata at the injection site (top left), but, as expected, not in distant motor cortex (M1, bottom left). Injection of Cre-inducible AAV5-EF1α::eNpHR3.0-EYFP into the ipsilateral motor cortex (M1) led to opsin expression (EYFP fluorescence) in M1 somata (bottom right), but, as expected, in S1, eNpHR3.0-EYFP was seen only in projecting axon terminals from these M1 cells (dispersed green puncta), not in somata (top right). Optrode recordings in vivo from the M1 site (560 nm light; bottom trace).

(E) The two dentate gyri were injected with AAV2-EF1a-mCherry-IRES-WGA-Cre (left) and AAV8-EF1a-DIO-ChR2-EYFP (right). Lower panels show high-magnification images of boxed regions above. Cells transduced with WGA-Cre expressed mCherry as expected (red), almost entirely within the granule cell layer (GCL) delineated by DAPI fluorescence (blue). WGA-Cre activated Cre-dependent opsin expression (EYFP fluorescence) in the contralateral hilus (arrowhead), a known source of projections to the ipsilateral dentate (note that on the contralateral side, EYFP fluorescence was confined to the hilus as expected; top right). This projection from the contralateral hilus is known to synapse on dentate granule cells in the molecular layer (Ratzliff et al., 2004), which in turn is visible as a thin green strip of opsin-EYFP expression bordering the GCL (ML, top left). Optrode extracellular recordings during optical stimulation (30 Hz, 5 ms, 473 nm) confirmed functional in vivo opsin expression in dentate neurons expressing ChR2-EYFP (bottom trace).

both eNpHR3.0 and eNpHR3.1 (a shorter version of eNpHR3.0 with equivalent functionality but the N-terminal signal peptide removed) (Figure 2A). A major in vivo opportunity for systems neurobiology would be controlling not just a projection from region A to region B, but a cell type itself that has (among its connections) a projection from A to B. This fundamentally distinct result requires multiplexing of optical control with other targeting methods (Figure 2B). Such control would be of great value in systems neurobiology; for example, cortical excitatory pyramidal neurons form a genetically and anatomically defined class of cell, but within this class are cells that each project to multiple different areas of the brain (e.g., thalamus, spinal cord, striatum, and other cortical areas) and therefore have fundamentally distinct roles (Lein et al., 2007; Yoshimura et al., 2005). It is unlikely that genetic tools will advance far enough to separate all of these different cell classes, pointing to the need to inhibit or excite cell types defined also by connection topology (Figure 2B).

One way to achieve this goal would be to capitalize on transcellular trafficking: to introduce into the local cell-body location a Cre-dependent virus conditionally expressing the microbial opsin gene of choice (e.g., Tsai et al., 2009), and rather than additionally employing a Cre-driver mouse line, to instead introduce into a distant target structure (chosen to define the cells of interest by anatomical connectivity) a virus expressing Cre recombinase fused to a transcellular tracer protein, e.g., wheat germ agglutinin (WGA) (Figure 2B) or tetanus toxin- fragment C (TTC) (Kissa et al., 2002; Maskos et al., 2002; Perreault et al., 2006; Sano et al., 2007; Sugita and Shiba, 2005). Cre recombinase in the fusion protein would be transported by presumed endosomal trafficking mechanisms along with the tracer to the local cell-body location if anatomically connected and activate opsin expression in the subset of local cells defined by this connectivity (Figure 2B). Note that this approach does not require any specific promoter fragment or genetic definition of target cells

(a clear advantage for use in less-genetically tractable species such as rats and primates), as with earlier projection-based targeting methods that are not transcellular (Gradinaru et al., 2007, 2009; Petreanu et al., 2007, 2009; Lima et al., 2009); but, if needed, such additional genetic refinements can be readily added (for example, both the WGA-Cre- and the Cre-dependent opsin could be delivered under control of cell type-specific promoters where available; Figure 2C), creating a potentially versatile means for addressing cells defined at the intersection of connectivity, location, and genetics.

We first validated this concept in the rat (Figure 2D) by devising a strategy to selectively introduce eNpHR3.0 into those primary motor cortex (M1) microcircuits that are involved in corticocortical connections with primary sensory cortex (S1) (Colechio and Alloway, 2009). To do this, we injected the previously described Cre-dependent AAV, now conditionally expressing eNpHR3.0 into motor cortex, and injected a novel WGA-Cre-expressing AAV (AAV2-EF1α-mCherry-IRES-WGA-Cre) remotely into primary somatosensory cortex. Robust eNpHR3.0-EYFP expression was indeed observed in a distributed subset of the motor cortex neurons (Figure 2D) at 5 weeks after injection, despite the remoteness of the Cre recombinase AAV injection; in control animals without Cre recombinase, no expression is observed from these Cre-dependent AAVs (Tsai et al., 2009; Sohal et al., 2009). Consistent with the anticipated mode of *trans*-synaptic or transcellular transport of Cre, no mCherry-positive cell bodies were observed in motor cortex, and no EYFP-positive cell bodies were observed in S1 sensory cortex (Figure 2D). The expected EYFP-eNpHR3.0 axon terminals arising from M1 were present in S1 (Figure 2D, top right). Simultaneous optrode stimulation/recording (Gradinaru et al., 2007) was conducted to validate functionality of eNpHR3.0 under the WGA system; indeed, robust inhibition was readily observed in M1 (trace in Figure 2D), as expected from the intense fluorescence of the XFP-opsin fusion protein.

To independently validate this targeting technology in a distinct circuit and with a different opsin, we next targeted hippocampal formation dentate gyrus neurons involved in interhemispheric projections (Figure 2E). Within the dentate hilus, the only known monosynaptic contralateral projection arises from the hilar mossy cells, which terminate on granule cells of the contralateral dentate, in dendrites of the molecular layer (Figure 2B) (Freund and Buzsáki, 1996; Ratzliff et al., 2004). The WGA-Cre AAV was unilaterally injected into one dentate gyrus, while the Cre-dependent AAV was injected into the contralateral dentate gyrus of the same animal. Strikingly, opsin expression was observed only in hilar cells of the contralateral side. Indeed, in this case and at this time point, contralateral dentate accumulation of Cre appeared to extend only to the hilus, as no EYFP labeling was observed in the contralateral granule cell layer (Figures 2B and 2E). Suggesting relatively little direct transduction of axon terminals with this AAV serotype, no mCherry was observed in the contralateral dentate (for cases wherein such direct transduction can and does occur, robust photosensitization of the incoming projection along with some reduced specificity of targeting with regard to postsynaptic cell type would be expected to result). The only EYFP-expressing circuit elements in the ipsilateral dentate, affording precise opportunities for optical control, were axonal fibers observed to terminate in the molecular layer of the granule cell layer, precisely as expected for fibers arising from the contralateral dentate hilus (Figures 2B and 2E). Indeed, in vivo optrode recordings confirmed the functionality of WGA/Cre-activated ChR2 in driving light-triggered spikes both at the opsin-expressing cell bodies (Figure 2E) and in neurons downstream to the axonal projections of ChR2-expressing cells, in the contralateral hemisphere (data not shown); in line with previous optogenetic studies (Zhang et al., 2007a; Gradinaru et al., 2007, 2009), 473 nm light pulses at 30 Hz (5 ms pulse width) delivered through the optical fiber reliably drove neuronal firing (Figure 2E) in vivo.

Far-Red Optogenetic Control

The utility of these targeting strategies for engineered opsins within intact tissue raised the question of whether additional advantages might be accrued with regard to volume of tissue modulatable in vivo. While membrane trafficking modifications alone will not shift the action spectrum, the capability to control neurons in the far red is a long-sought goal of optogenetics, as this will allow use of light that penetrates much more deeply into scattering biological tissues (as with the far-red utility recently demonstrated for fluorescent proteins) (Shu et al., 2009), and therefore will allow recruitment of larger volumes (Aravanis et al., 2007; Adamantidis et al., 2007; Gradinaru et al., 2009). The massive photocurrents observed for eNpHR3.0 ($\sim$20× those initially reported for NpHR, which itself is capable of blocking spiking in response to 589 nm amber light), suggested optogenetic control with far-red light might be achieved. We therefore explored optical control in the far red with the trafficking-enhanced eNpHR3.0.

Even in response to true-red (630 nm) light of only 3.5 mW/mm^2, we observed potent $\sim$250 pA outward photocurrents in virally transduced cells—still more than 6-fold larger than the first-observed NpHR currents with yellow light (Figure 3A), and maintaining the characteristic step-like, stable kinetics typical of NpHR (Zhang et al., 2007a) (Figure 1; Figure S1). Moreover, we found that these photocurrents evoked by red light could be used to trigger large (>40 mV) hyperpolarizations in hippocampal pyramidal neurons (Figure 3B). We therefore explored even further red-shifted light. We continued to observe robust photocurrents in the deep red with 660 nm light and at the red/infrared border with 680 nm light (Figure 3C). Importantly, at all of the red and far-red wavelengths tested, eNpHR3.0 photocurrents readily blocked action potentials induced by current injection (Figure 3D) with 7 mW/mm^2 or less, validating the extension of optogenetic control channels to far-red light.

One important feature of NpHR is its spectral compatibility with ChR2: the two opsins have largely separable action spectra and operate with similar light power density requirements, allowing bidirectional control of optical activity (Zhang et al., 2007a) in vitro or in vivo despite a small region of spectral overlap. To test whether eNpHR3.0 had become too potent, given the spectral overlap, to use in combination with ChR2 in the same cell, we created a bicistronic vector containing eNpHR3.0; analogous 2A-based combination vectors (Ryan and Drew, 1994) have been employed with earlier tools, and channelrhodopsin currents with this method have ranged from 150 to 240 pA and

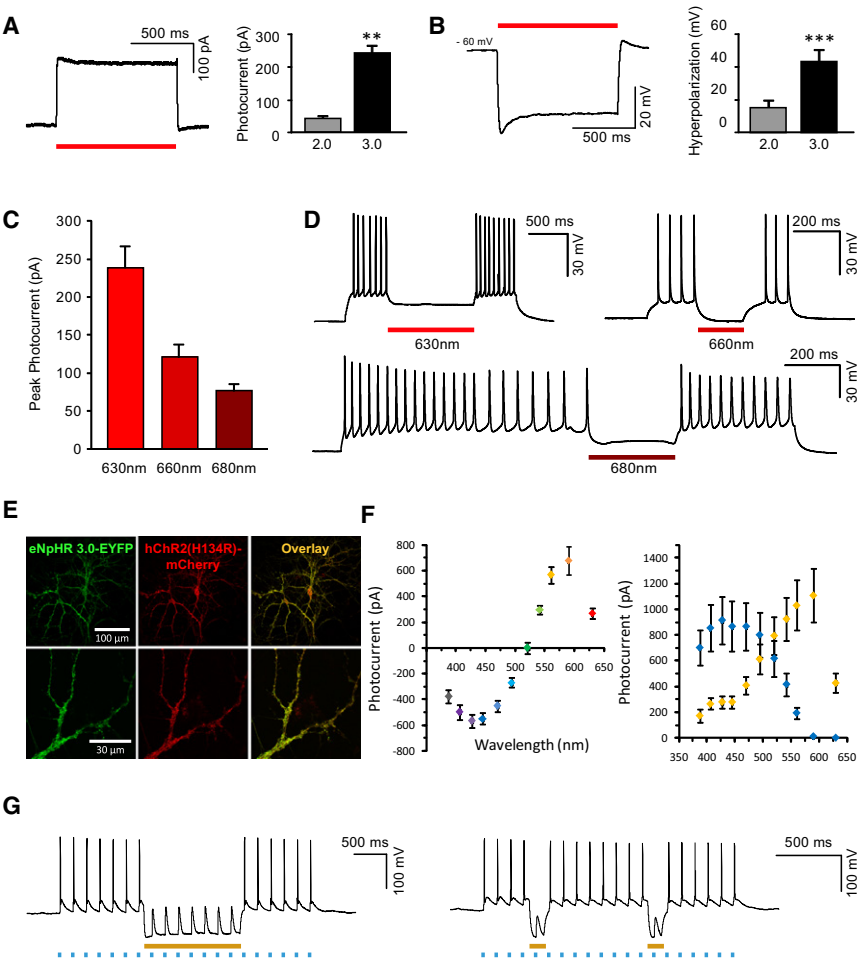

Figure 3. Far-Red Optogenetic Inhibition and Single-Component, Bidirectional Optical Control

(A) Six hundred thirty nanometer light evokes robust photocurrents in neurons transduced with eNpHR3.0 (representative voltage clamp trace at left). Summary plot comparing eNpHR2.0- and eNpHR3.0-expressing neurons (at right); eNpHR2.0, 42.7 ± 4.5 pA; eNpHR3.0, 239.4 ± 28.7 pA; unpaired t test p = 0.00004; n = 10).

(B) Six hundred thirty nanometer illumination evoked robust hyperpolarization (representative voltage clamp trace at left). Summary plot comparing eNpHR2.0- and eNpHR3.0-expressing neurons (right); 15.6 ± 3.2 mV for eNpHR2.0 and 43.3 ± 6.1 mV for eNpHR3.0; unpaired t test p = 0.00116; n = 10).

(C) Summary of outward photocurrents evoked by different wavelengths of red and far-red/infrared border illumination: 630 nm, 239.4 ± 28.7 pA (left, n = 10); 660 nm, 120.5 ± 16.7 pA (middle, n = 4); and 680 nm: 76.3 ± 9.1 pA (right, n = 4). Power density: 3.5 mW/mm^2 (630 nm) and 7 mW/mm^2 (660 nm, 680 nm).

(D) Illumination with red and far-red/infrared border light inhibited spiking induced by current injection in neurons expressing eNpHR3.0. Typical current-clamp traces show optical inhibition at 630 nm (top left), 660 nm (top right), and 680 nm (bottom). Power density: 3.5 mW/mm^2 (630 nm) and 7 mW/mm^2 (660 nm, 680 nm).

(E) eNpHR 3.0-EYFP (left) and hChR2-mCherry (middle) expressed both on the neuronal membrane and throughout the neurites.

(F) Activation spectrum for eNPAC (left), and for ChR2(H134R) (right, blue) and eNpHR3.0 (right, yellow) alone. Maximum eNPAC steady-state excitation was 567 ± 49 pA at 427 nm (n = 9), 62% of the value for ChR2(H134R) alone (916 ± 185 pA; n = 5). Similarly, maximum eNPAC inhibition was 679 ± 109 pA at 590 nm (n = 9), 61% of the value for eNpHR3.0 alone (1110 ± 333 pA; n = 4). Output power density for peak eNpHR3.0 current values was 3.5–5 mW/mm^2 (3.5 mW/mm^2 at 590 nm).

(G) Blue light (445 nm, 5 ms pulses) drove spiking at 20 Hz (left) and 10 Hz (right), while simultaneous application of yellow light (590 nm) inhibited spikes.

halorhodopsin currents from 11 to 40 pA (Tang et al., 2009, Han et al., 2009b). We transfected the eNpHR3.0-2A-ChR2 construct (abbreviated eNPAC) into hippocampal pyramidal neurons. Figure 3E shows that trafficking of both opsin gene products to cellular processes was observed. To verify that independent excitation and inhibition was still possible despite the increased currents from eNpHR3.0, we mapped out the steady-state photocurrent action spectrum in detail for eNPAC and for ChR2(H134R) (Gradinaru et al., 2007) and eNpHR3.0 alone (Figure 3F). Maximal eNPAC steady-state excitatory and inhibitory currents were both approximately 60% of that observed when each opsin was expressed individually, yielding maximal photocurrents of >550 pA in each direction (Figures 3F and 3G); the modestly overlapping action spectra may provide a feature, in that potent shunting inhibition combined with hyperpolarizing inhibition is likely possible with this combination approach. Validation in vivo will require demonstration that the specific P2A method (or other linker approach) is functional in a particular circuit or cell type (yet to be determined); however, these data in cultured hippocampal neurons demonstrate that potent bidirectional photocurrents of >500 pA each can be achieved within a single cell, without incapacitating interference of the trafficking-enhanced opsin.

Optical Inhibition in the Green and Blue Enabled by Cellular and Genomic Tools

The known wide action spectrum of the microbial opsins (Figure 3) poses challenges with regard to achieving multiple independent channels of control; interestingly, eNpHR3.0 becomes not only a potent far-red optical control tool, but also the most potent known blue light-driven opsin-based inhibitor (>400 pA at 472 nm; Figure 3F). Indeed, the membrane trafficking strategies delineated here may form a generalizable strategy for adapting diverse microbial opsins with unique properties for optogenetic control purposes. In a final series of experiments, we explored whether these and other enhanced membrane trafficking principles could enable the addition of genetically and functionally distinct components to the optogenetic toolbox.

While a very large number of microbial opsins genes exist in nature, we and others have thus far found none that outperform

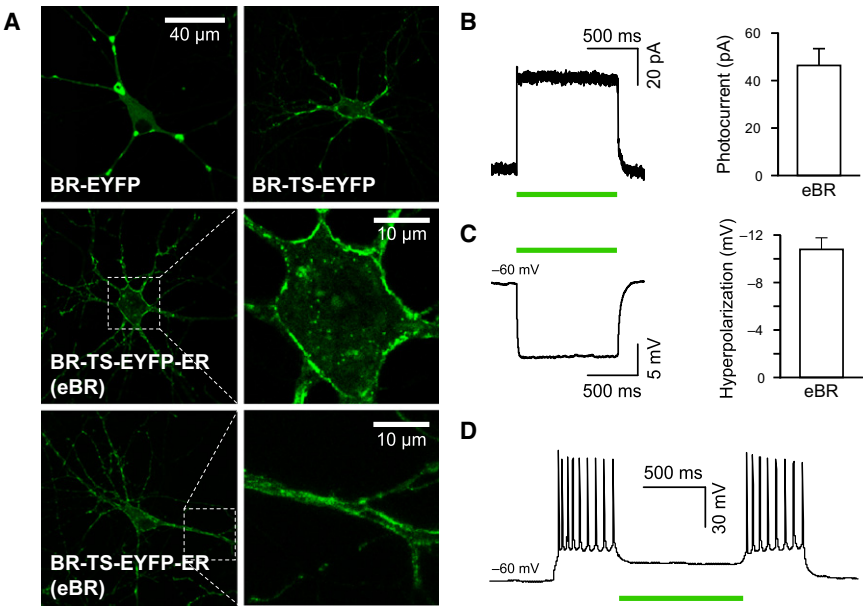

Figure 4. eBR: Trafficking-Enhanced Tool for Green Inhibition

(A) Confocal images in hippocampal neurons: unmodified BR forms aggregates similar to those of unmodified NpHR (top left). Provision of the TS motif before EYFP decreased aggregate size but did not fully eliminate aggregates (top right). Only when the ER export motif (FCYENEV) was also added to the C terminus were aggregates abolished, resulting in good membrane targeting throughout the soma (middle panels) and far into processes (bottom panels).

(B) Five hundred sixty nanometer light (green bar) induced outward photocurrents in eBR cells (left, sample trace in voltage clamp), 46.4 ± 7.2 pA (right bar graph). Mean ± SEM is plotted, n = 12. Membrane input resistance was similar for all neurons patched (131.6 ± 19.5 mΩ). Light power density at sample was 7 mW/mm^2.

(C) Corresponding light-induced hyperpolarizations (left, sample trace in current clamp) were 10.8 ± 1.0 mV (right bar graph). Mean ± SEM is plotted, n = 12.

(D) Illumination with green light (560 nm) sufficed to inhibit current injection-induced spiking.

See also Figure S2.

eNpHR3.0 (as described herein) with regard to photocurrent size, light requirements, or kinetics (Zhang et al., 2007a; Han and Boyden, 2007; Chow et al., 2010). It is important to continue to expand the optogenetic toolbox, but we have found that most microbial opsins traffic poorly in mammalian cells (Figure 4; Figure S2). However, application of the trafficking principles for microbial opsin engineering outlined here may enable optogenetics to continue the genomics progress over the past few years (Zhang et al., 2008), capitalizing on the immense natural diversity of microbial opsins (Zhang et al., 2008; Chow et al., 2010). We sought to test the adaptability of the membrane trafficking principle with the best-characterized microbial opsin, bacteriorhodopsin (BR) (Stoeckenius and Bogomolni, 1982), from *H. salinarum*, a green light-activated regulator of transmembrane ion conductance (Marti et al., 1991).

We found that expressed in unmodified form, prominent intracellular accumulations were observed, similar to those seen when the *Natronomonas* halorhodopsin is expressed at high levels (Figure 4A, top left), and no photocurrents were observed. However, addition of the trafficking signal (TS, as employed for eNpHR3.0) between BR and EYFP substantially improved membrane and process localization (Figure 4A, top right), with smaller persistent ER-like accumulations that were eliminated with further C-terminal addition of the ER export signal FCYENEV (Figure 4A, center row). The resulting construct (eBR, doubly engineered for optimal membrane trafficking) was well tolerated in cultured neurons, with marked membrane localization and process targeting (Figure 4A, center right and bottom row). Validation of functional plasma membrane targeting revealed that eBR could typically deliver ~50 pA of outward photocurrent (Figure 4B) and ~10 mV hyperpolarizations (Figure 4C) that sufficed to block spiking in hippocampal pyramidal neurons when exposed to the optimal wavelength light of 560 nm (Figure 4D), thereby providing another channel for optogenetic control and illustrating the potential generalizeability of the microbial opsin membrane trafficking approach.

We also continued genomic strategies similar to those that allowed our identification of the red-shifted excitatory opsin VChR1 from *Volvox carteri* (Zhang et al., 2008); indeed, a number of microbes have been reported to display light sensitivities from violet to near infrared. We accordingly continued our broad genomic mining approach in environmental sequencing databases, plant/microbial expressed sequence tag (EST) libraries, and whole-genome shotgun (WGS) sequencing repositories to search for new rhodopsins with channel or pump properties and novel light sensitivities (Zhang et al., 2008). Using the primary amino acid sequences for ChRs, HRs, and BRs as the template sequence, we continued the search among evolutionarily distant species (Zhang et al., 2008; Chow et al., 2010). Among other candidate sequences from diverse hosts (*Cryptomonas*, *Guillardia*, *Mesostigma*, *Dunaliella*, *Gloeobacter*, etc.), one of these from *Guillardia theta* was different from the previously reported GtR1 and GtR2 (Sineshchekov et al., 2005) and showed high amino acid homology to ChR2. We designated this new protein as *G. theta* rhodopsin-3 (GtR3, Figure S2A), optimized the codon bias of GtR3 for mammalian expression, and delivered the GtR3-EYFP fusion gene to hippocampal pyramidal neurons. In an emerging theme, GtR3 showed intracellular accumulations (Figure S2B, left) and no photocurrents. Provision of the TS signal between GtR3 and EYFP only mildly reduced accumulations (Figure S2B, middle), but, together with addition of the ER export signal FCYENEV to the C terminus (Figure S2B, right), accumulations were abolished and increased surface and process localization observed. The resulting modified GtR3 hyperpolarizes hippocampal neurons (Figure S2C, left) in response to 472 nm blue light, albeit with smaller currents than eBR (Figure S2C, right), and could inhibit spiking as well (Figure S2D). We also achieved blue inhibition of spiking with

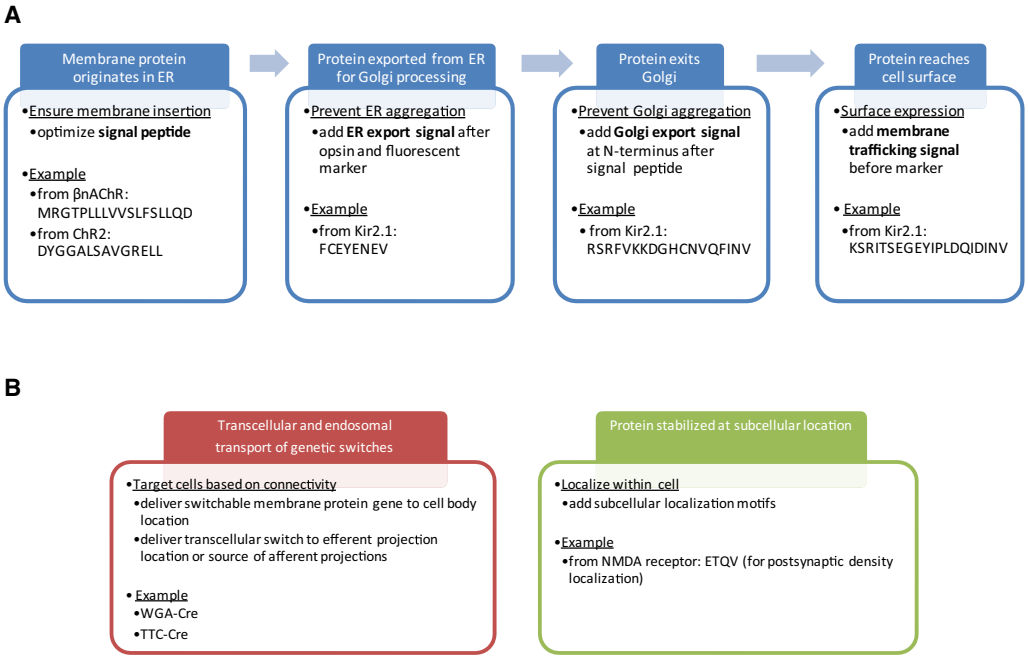

Figure 5. Optogenetics: Molecular Design for Microbial Tools

(A) General subcellular targeting strategies for adapting microbial opsin genes to metazoan intact-systems biology.

(B) Refinement of targeting at the tissue and subcellular levels. Subcellular opsin targeting methods have been previously described (for various dendritic compartment strategies, see Gradinaru et al. [2007] and Lewis et al., [2009]), and tissue/transcellular opsin targeting methods are described in Figure 2.

an opsin (AR) from *Acetabularia acetabulum* (Tsunoda et al., 2006; Chow et al., 2010) engineered for improved trafficking; AR generates little current alone but was initially aggregate free and required only addition of the TS signal between AR and EYFP for functional membrane localization and spike inhibition (Figure S2E).

While these and other published microbial opsin-derived inhibitors are not yet as potent as eNpHR3.0 (and for this reason we continue with eNpHR3.0 for optogenetic applications), the improved functionality achieved here by membrane trafficking modifications point to the potential versatility of this approach in unlocking the full potential of ecological diversity, and to the individualized strategies that will be indicated for different microbial opsin genes (Figure 5).

DISCUSSION

Single-component optogenetic approaches previously have found substantial utility in the control of biological processes and behavior in freely moving mammals (Adamantidis et al., 2007; Airan et al., 2009; Gradinaru et al., 2009; Petreanu et al., 2007, 2009; Sohal et al., 2009; Tsai et al., 2009) and other animals (Douglass et al., 2008; Hwang et al., 2007; Zhang et al., 2007a), with the high temporal precision that is important for intact-systems biology. We have found that engineering specific membrane-trafficking capabilities for microbial proteins is an important step in generating diverse optogenetic technologies for intact-systems biology. Not all trafficking strategies will be suitable for all microbial opsins, with different motifs required for opsins that encounter trafficking difficulty at different stages; therefore, careful subcellular analysis with rational selection of proper modifications together constitute a directed and principled strategy that may be applicable to all opsins of non-mammalian origin, thereby enabling systematic generation of novel optogenetic tools from genomic resources (Figure 5).

eNpHR3.0: New Quantitative Properties and New Classes of Application

We have previously observed that inhibition with NpHR and NpHR2.0, while useful for many applications (Gradinaru et al., 2009; Sohal et al., 2009; Tønnesen et al., 2009; Arrenberg et al., 2009), can in some cases be overcome by very strong excitation (Sohal et al., 2009). Hyperpolarizations by greater than 100 mV (Figure 1) with eNpHR3.0 provide a substantial step forward in the potency of optical inhibition. The inhibition now provided with eNpHR3.0, more than 20-fold stronger than the initial NpHR, remains tunable with light intensity or duty-cycle adjustments, as with any of the optogenetic tools. At the action spectrum peak, nanoampere-scale mean outward currents readily resulted (Figure 3F, right) with only 3.5 mW/mm^2 yellow light (10-fold less light power than required for approaching similar currents with previously described proton pumps). At the same time, eNpHR3.0 preserved the step-like kinetics, fast recovery, and resistance to inactivation over long timescales of NpHR (Zhang et al., 2007a) (Figure S1; Figures 1 and 3).

eNpHR3.0 is particularly well suited for in vivo applications, as the most red-shifted and potent optogenetic inhibitor to date, but further strategies to enhance potency of this and other tools will

no doubt emerge, and membrane trafficking work as described here may enable even more potent inhibitors in the future. When employing eNpHR3.0, inhibition can be readily dialed down if needed by using weaker promoters, shorter expression times, or reduced light levels, while maintaining access to new wavelengths ~100 nm red-shifted from previous reports (680 nm versus 589 nm; Figure 3) to enable operating at the infrared border with deeper-penetrating and safer photons. Of course, not only the opsin gene and light source selected, but also the strategy for circuit element targeting, may determine effectiveness; for example, optogenetic work on Parkinsonian models (Gradinaru et al., 2009) showed that therapeutically effective deep brain stimulation (DBS) in the subthalamic nucleus (STN) is likely initiated by action on afferent axons (which in turn then modulate both downstream and upstream networks). While direct fiberoptic-based inhibition of local cell bodies in the STN did not show behavioral effects comparable to those observed with direct modulation of afferent axons, these results do not mean that inhibition of the STN is not important (indeed, optogenetic axonal modulation in the STN results in inhibition of STN spiking, as noted by Gradinaru et al. [2009]). Rather, these results informed the long-standing clinical significant questions surrounding the mechanism and target of DBS by showing that axonal modulation constitutes the likely therapeutic mechanism and a highly efficient means for a point source such as a DBS electrode (or optical fiber) to control a structure or network in diseased neural circuitry (Gradinaru et al., 2009). In addition to these circuit element targeting considerations, the light intensity and wavelength, promoter choice, virus titer, virus tropism, time of opsin expression, target cell biophysics, and local patterns of endogenous activity and modulation will all affect optogenetic inhibition efficacy and should be carefully considered for each experimental system (Cardin et al., 2010; Zhang et al., 2010).

Tissue-Topology Targeting for Optogenetics

To enable control of cell types on the basis of connectivity properties, we developed a Cre recombinase-based two-virus strategy (Figure 2) in which cells were targeted with well-tolerated AAV methods without use of cell type-specific promoter fragments or transgenic animals. In each system, this approach must be validated for directionality (antero- or retrograde) and extent of Cre transport, which may depend on cell-specific endosomal dynamics and experimental timepoint; this strategy may also work only with viruses rather than mouse transgenesis, allowing Cre access to episomal DNA. The dual-virus approach described here capitalizes upon the high efficiency and long-term tolerability of AAVs while also enabling robust optical control (Figures 2D and 2E) via catalytically driven activation of high copy-number transgenes. It is important to be aware that direct transduction of axon terminals with certain viruses can be achieved for targeting (reviewed in Callaway, 2008), and indeed virtually all viruses (including AAVs) carry some degree of this capability in a serotype- and circuit-dependent manner, as we and others have observed (Burger et al., 2004; Paterna et al., 2004; Callaway, 2008; Lima et al., 2009; Passini et al., 2005; Nathanson et al., 2009). It is also important to consider (in the process of selecting viruses) the need for high levels of infection and expression while avoiding adverse effects on transduced neurons over weeks to months for long-term electrophysiological or behavioral experiments.

As shown in Figure 2, the cell-process targeting enabled by membrane trafficking modification allows for control of cells that are defined topologically—that is, by the essential character of their connections within tissue. At present, it is not guaranteed that transport is synaptic or monosynaptic (as in the hippocampal circuit experiments in Figure 2, such properties will need to be validated in each system); therefore, the term "topological targeting" rather than synaptic targeting is here used to underscore the deformation independence of the fundamental character of the connection—an axonal connection can take any path from A to B, and as long as the connection is present, the topological targeting strategy remains valid. This property is important in genetically less-tractable organisms, but also of substantial value even in animals such as mice, where genetic targeting tools are in many cases inadequate. Of course, genetic targeting strategies may be multiplexed with topological targeting; for example, expression from the Cre-dependent vector and the Cre-fusion vector (Figure 2C) may each be governed by specific genetic targeting sequences if available. Moreover, the availability of multiple channels of optical control opens the door to combinatorial topological targeting strategies.

Avenues for Technology Development and Application

Like ChR2, NpHR, and VChR1, we note that most microbial opsins can benefit from substantial protein engineering to achieve new kinds of functionality. Indeed, we and others have previously demonstrated molecular strategies for eliciting from microbial opsins increased light sensitivity (Berndt et al., 2009), increased photocurrent magnitude (Gradinaru et al., 2007, 2008; Zhao et al., 2008), faster kinetics (Gunaydin et al., 2010; Lin et al., 2009), and bistable switching behavior (Berndt et al., 2009). Other possibilities such as shifted action spectrum (Zhang et al., 2008; Gunaydin et al., 2010), increased two-photon responsivity, and altered ion permeability (e.g., for Ca^{2+}) may also be achieved in the future.

While ion conductance-regulating opsins have been the most versatile for ready translation (employing a common electrical language), biochemical control with light in defined cell types is also possible (but with a different set of approaches, given that microbial signal transduction employs principles distinct from metazoan signaling). Indeed, optogenetic control of well-defined biochemical signaling pathways was recently achieved both in cultured cells and in freely moving mammals, using the optoXR method for optical control of specified G protein-coupled receptor signaling (Airan et al., 2009). A photoactivatable adenylyl cyclase has been studied from Euglena, although with high dark activity that limits in vivo application (Schröder-Lang et al., 2007), and subsequent work on light-sensitive PAS or LOV domains (Levskaya et al., 2009; Wu et al., 2009) may open up new ways to control protein-protein association if these approaches can be made to operate in living animals.

We have found that in the nervous system, optogenetic tools can be applied to probe the neural circuit underpinnings of information transmission, oscillations, locomotion, awakening, and reward, as well as to probe the operation of neural circuits

important in a number of brain diseases including Parkinson's disease and epilepsy (Adamantidis et al., 2007; Airan et al., 2009; Cardin et al., 2009; Gradinaru et al., 2009; Sohal et al., 2009; Tønnesen et al., 2009; Tsai et al., 2009). Moroever, results thus far point to substantial versatility of the optogenetic approach across animal species (Adamantidis et al., 2007; Airan et al., 2009; Aravanis et al., 2007; Arenkiel et al., 2007; Bi et al., 2006; Boyden et al., 2005; Chow et al., 2010; Douglass et al., 2008; Gradinaru et al., 2008, 2009; Hägglund et al., 2010; Han et al., 2009a; Huber et al., 2008; Hwang et al., 2007; Ishizuka et al., 2006; Li et al., 2005; Nagel et al., 2003; Petreanu et al., 2007, 2009; Tsai et al., 2009; Wang et al., 2007; Zhang et al., 2006, 2007a; Zhang and Oertner, 2007; Zhao et al., 2008). Together with fiberoptic (Adamantidis et al., 2007; Aravanis et al., 2007) and integrated fiberoptic-electrode "optrode" assemblies (Gradinaru et al., 2007), even cells located deep within large, dense organs can be readily accessed and interrogated in freely moving mammals. The additional resources defined here arise from the application of molecular, cellular, and genomic strategies to enable expansion of the capabilities of optical control, and, as this toolbox rapidly grows, optogenetics may come to play an increasingly potent and versatile role in intact-systems biology for the fast control of defined cells within functioning tissues.

EXPERIMENTAL PROCEDURES

Constructs

All NpHR variants were produced by PCR amplification of the NpHR-EYFP construct previously published (Zhang et al., 2007a). All opsins described here have been optimized for mammalian expression by changing each gene's codon usage to conform to human codon usage distribution. Updated maps and vectors are freely distributed from the Deisseroth laboratory and described at http://www.optogenetics.org/.

Hippocampal Cultures

Primary cultured hippocampal neurons were prepared from P0 Sprague-Dawley rat pups. The CA1 and CA3 regions were isolated, digested with 0.4 mg/ml papain (Worthington, Lakewood, NJ), and plated onto glass coverslips precoated with 1:30 Matrigel (Beckton Dickinson Labware, Bedford, MA) at a density of 65,000/cm^2. Hippocampal cultures grown on coverslips were transfected or transduced at 4 days in vitro (DIV) with titer-matched viruses for all constructs (final dilution 10^4 infectious units (i.u.)/ml in neuronal growth medium). Whole-cell patch clamp recordings were performed as previously described (Zhang et al., 2007a). At 14 DIV, cultures were fixed for 30 min with ice-cold 4% paraformaldehyde and then permeabilized for 30 min with 0.4% saponin in 2% normal donkey serum (NDS). Primary antibody incubations were performed overnight at 4°C; Cy3-conjugated secondary antibodies (Jackson Laboratories, West Grove, PA) were applied in 2% NDS for 1 hr at room temperature. Images were obtained on a Leica confocal microscope with a 63×/1.4 NA oil objective.

Stereotactic Injection into the Rodent Brain and Optrode Recordings

Adult mice and Long-Evans rats were housed according to the approved protocols at Stanford. All surgeries were performed under aseptic conditions. The animals were anesthetized with intraperitoneal injections of a ketamine (80 mg/kg)/xylazine (15–20 mg/kg) cocktail (Sigma). The virus was delivered via a 10 μl syringe and a thin 34 gauge metal needle; the injection volume and flow rate (1 μl at 0.1 μl/min) were controlled with an injection pump from World Precision Instruments (Sarasota, FL). For validation of opsin functionality, simultaneous optical stimulation and electrical recording in living rodents was conducted as described previously (Gradinaru et al., 2007) with an optrode composed of an extracellular tungsten electrode (1 MΩ, ~125 μm) attached to an optical fiber (~200 μm) with the tip of the electrode deeper (~0.4 mm) than the tip of the fiber to ensure illumination of the recorded neurons. The optical fiber was coupled to a 473 nm (for ChR2) or 560 nm (for eNpHR3.0) laser diode (10 mW fiber output) from CrystaLaser. Optrode recordings were conducted in rodents anesthetized with 1.5% isoflurane, and the optode was placed through small craniotomies created above target regions. pClamp 10 and a Digidata 1322A board were used to both collect data and generate light pulses through the fiber. The recorded signal was band-pass filtered at 300 Hz low/5 kHz high (1800 Microelectrode AC Amplifier).

Tissue Slice Preparation

For preparation of brain slices, mice or rats were sacrificed 4 to 5 weeks after viral injection. Rodents were perfused with 20 ml ice-cold PBS, followed by 20 ml 4% paraformaldehyde. The brains were then fixed overnight in 4% paraformaldehyde and transferred to 30% sucrose solution for 2 days. Brains were frozen and coronal slices (40 μm) were prepared with a Leica SM2000R cryostat and preserved in 4°C in cryoprotectant (25% glycerol and 30% ethylene glycol in PBS). Slices (DAPI stain 1:50,000) were mounted with PVA-DABCO on microscope slides, and single confocal optical sections (e.g., through dorsal CA1 region, ~1–2.5mm posterior to bregma or the dorsal subiculum, 2.7–3 mm posterior to bregma) were acquired using a 10× air and 40×/1.4 NA oil objectives on a Leica confocal microscope.

SUPPLEMENTAL INFORMATION

Supplemental Information includes Extended Experimental Procedures and two figures and can be found with this article online at doi:10.1016/j.cell.2010.02.037.

ACKNOWLEDGMENTS

V.G. is supported by the Stanford Interdisciplinary Graduate Fellowship, F.Z. by the National Institutes of Health (NIH) and Harvard Society of Fellows, J.M. by the Stanford Medical Scientist Training Program, R.P. by the NIH, I.D. by the German Academic Exchange Service and the Human Frontier Science Program, I.G. by the Machiah Foundation and the Weizmann Institute, K.T. by the National Alliance for Research on Schizophrenia and Depression, and K.D. by the Woo, Keck, Snyder, McKnight, Yu, and Coulter Foundations, as well as by the California Institute of Regenerative Medicine, the National Science Foundation, and the NIH. We thank the entire Deisseroth lab for their support.

Received: October 9, 2009
Revised: January 11, 2010
Accepted: February 18, 2010
Published online: March 18, 2010

REFERENCES

Adamantidis, A.R., Zhang, F., Aravanis, A.M., Deisseroth, K., and de Lecea, L. (2007). Neural substrates of awakening probed with optogenetic control of hypocretin neurons. Nature *450*, 420–424.

Airan, R.D., Thompson, K.R., Fenno, L.E., Bernstein, H., and Deisseroth, K. (2009). Temporally precise in vivo control of intracellular signalling. Nature *458*, 1025–1029.

Aravanis, A.M., Wang, L.P., Zhang, F., Meltzer, L.A., Mogri, M.Z., Schneider, M.B., and Deisseroth, K. (2007). An optical neural interface: in vivo control of rodent motor cortex with integrated fiberoptic and optogenetic technology. J. Neural Eng. *4*, S143–S156.

Arenkiel, B.R., Peca, J., Davison, I.G., Feliciano, C., Deisseroth, K., Augustine, G.J., Ehlers, M.D., and Feng, G. (2007). In vivo light-induced activation of neural circuitry in transgenic mice expressing channelrhodopsin-2. Neuron *54*, 205–218.

Arrenberg, A.B., Del Bene, F., and Baier, H. (2009). Optical control of zebrafish behavior with halorhodopsin. Proc. Natl. Acad. Sci. USA *106*, 17968–17973.

Berndt, A., Yizhar, O., Gunaydin, L.A., Hegemann, P., and Deisseroth, K. (2009). Bi-stable neural state switches. Nat. Neurosci. *12*, 229–234.

Bi, G.Q., and Poo, M.M. (1998). Synaptic modifications in cultured hippocampal neurons: dependence on spike timing, synaptic strength, and postsynaptic cell type. J. Neurosci. *18*, 10464–10472.

Bi, A., Cui, J., Ma, Y.P., Olshevskaya, E., Pu, M., Dizhoor, A.M., and Pan, Z.H. (2006). Ectopic expression of a microbial-type rhodopsin restores visual responses in mice with photoreceptor degeneration. Neuron *50*, 23–33.

Boyden, E.S., Zhang, F., Bamberg, E., Nagel, G., and Deisseroth, K. (2005). Millisecond-timescale, genetically targeted optical control of neural activity. Nat. Neurosci. *8*, 1263–1268.

Burger, C., Gorbatyuk, O.S., Velardo, M.J., Peden, C.S., Williams, P., Zolotukhin, S., Reier, P.J., Mandel, R.J., and Muzyczka, N. (2004). Recombinant AAV viral vectors pseudotyped with viral capsids from serotypes 1, 2, and 5 display differential efficiency and cell tropism after delivery to different regions of the central nervous system. Mol. Ther. *10*, 302–317.

Callaway, E.M. (2008). Transneuronal circuit tracing with neurotropic viruses. Curr. Opin. Neurobiol. *18*, 617–623.

Cardin, J.A., Carlén, M., Meletis, K., Knoblich, U., Zhang, F., Deisseroth, K., Tsai, L.H., and Moore, C.I. (2009). Driving fast-spiking cells induces gamma rhythm and controls sensory responses. Nature *459*, 663–667.

Cardin, J.A., Carlén, M., Meletis, K., Knoblich, U., Zhang, F., Deisseroth, K., Tsai, L.H., and Moore, C.I. (2010). Targeted optogenetic stimulation and recording of neurons in vivo using cell-type-specific expression of Channelrhodopsin-2. Nat. Protoc. *5*, 247–254.

Chow, B.Y., Han, X., Dobry, A.S., Qian, X., Chuong, A.S., Li, M., Henninger, M.A., Belfort, G.M., Lin, Y., Monahan, P.E., and Boyden, E.S. (2010). High-performance genetically targetable optical neural silencing by light-driven proton pumps. Nature *463*, 98–102.

Colechio, E.M., and Alloway, K.D. (2009). Differential topography of the bilateral cortical projections to the whisker and forepaw regions in rat motor cortex. Brain Struct. Funct. *213*, 423–439.

Deisseroth, K., Feng, G., Majewska, A.K., Miesenböck, G., Ting, A., and Schnitzer, M.J. (2006). Next-generation optical technologies for illuminating genetically targeted brain circuits. J. Neurosci. *26*, 10380–10386.

Douglass, A.D., Kraves, S., Deisseroth, K., Schier, A.F., and Engert, F. (2008). Escape behavior elicited by single, channelrhodopsin-2-evoked spikes in zebrafish somatosensory neurons. Curr. Biol. *18*, 1133–1137.

Fleischmann, A., Shykind, B.M., Sosulski, D.L., Franks, K.M., Glinka, M.E., Mei, D.F., Sun, Y., Kirkland, J., Mendelsohn, M., Albers, M.W., and Axel, R. (2008). Mice with a "monoclonal nose": perturbations in an olfactory map impair odor discrimination. Neuron *60*, 1068–1081.

Freund, T.F., and Buzsáki, G. (1996). Interneurons of the hippocampus. Hippocampus *6*, 347–470.

Gradinaru, V., Thompson, K.R., Zhang, F., Mogri, M., Kay, K., Schneider, M.B., and Deisseroth, K. (2007). Targeting and readout strategies for fast optical neural control in vitro and in vivo. J. Neurosci. *27*, 14231–14238.

Gradinaru, V., Thompson, K.R., and Deisseroth, K. (2008). eNpHR: a Natronomonas halorhodopsin enhanced for optogenetic applications. Brain Cell Biol. *36*, 129–139.

Gradinaru, V., Mogri, M., Thompson, K.R., Henderson, J.M., and Deisseroth, K. (2009). Optical deconstruction of parkinsonian neural circuitry. Science *324*, 354–359.

Gunaydin, L.A., Yizhar, O., Berndt, A., Sohal, V.S., Deisseroth, K., and Hegemann, P. (2010). Ultrafast optogenetic control. Nat. Neurosci. *13*, 387–392.

Hägglund, M., Borgius, L., Dougherty, K.J., and Kiehn, O. (2010). Activation of groups of excitatory neurons in the mammalian spinal cord or hindbrain evokes locomotion. Nat. Neurosci. *13*, 246–252.

Han, X., and Boyden, E.S. (2007). Multiple-color optical activation, silencing, and desynchronization of neural activity, with single-spike temporal resolution. PLoS ONE *2*, e299.

Han, X., Qian, X., Bernstein, J.G., Zhou, H.H., Franzesi, G.T., Stern, P., Bronson, R.T., Graybiel, A.M., Desimone, R., and Boyden, E.S. (2009a). Millisecond-timescale optical control of neural dynamics in the nonhuman primate brain. Neuron *62*, 191–198.

Han, X., Qian, X., Stern, P., Chuong, A.S., and Boyden, E.S. (2009b). Informational lesions: optical perturbation of spike timing and neural synchrony via microbial opsin gene fusions. Front Mol Neurosci *2*, 12.

Hofherr, A., Fakler, B., and Klöcker, N. (2005). Selective Golgi export of Kir2.1 controls the stoichiometry of functional Kir2.x channel heteromers. J. Cell Sci. *118*, 1935–1943.

Huber, D., Petreanu, L., Ghitani, N., Ranade, S., Hromádka, T., Mainen, Z., and Svoboda, K. (2008). Sparse optical microstimulation in barrel cortex drives learned behaviour in freely moving mice. Nature *451*, 61–64.

Hwang, R.Y., Zhong, L., Xu, Y., Johnson, T., Zhang, F., Deisseroth, K., and Tracey, W.D. (2007). Nociceptive neurons protect Drosophila larvae from parasitoid wasps. Curr. Biol. *17*, 2105–2116.

Ishizuka, T., Kakuda, M., Araki, R., and Yawo, H. (2006). Kinetic evaluation of photosensitivity in genetically engineered neurons expressing green algae light-gated channels. Neurosci. Res. *54*, 85–94.

Kalaidzidis, I.V., Kalaidzidis, Y.L., and Kaulen, A.D. (1998). Flash-induced voltage changes in halorhodopsin from Natronobacterium pharaonis. FEBS Lett. *427*, 59–63.

Kissa, K., Mordelet, E., Soudais, C., Kremer, E.J., Demeneix, B.A., Brûlet, P., and Coen, L. (2002). In vivo neuronal tracing with GFP-TTC gene delivery. Mol. Cell. Neurosci. *20*, 627–637.

Lanyi, J.K., and Oesterhelt, D. (1982). Identification of the retinal-binding protein in halorhodopsin. J. Biol. Chem. *257*, 2674–2677.

Lein, E.S., Hawrylycz, M.J., Ao, N., Ayres, M., Bensinger, A., Bernard, A., Boe, A.F., Boguski, M.S., Brockway, K.S., Byrnes, E.J., et al. (2007). Genome-wide atlas of gene expression in the adult mouse brain. Nature *445*, 168–176.

Levskaya, A., Weiner, O.D., Lim, W.A., and Voigt, C.A. (2009). Spatiotemporal control of cell signalling using a light-switchable protein interaction. Nature *461*, 997–1001.

Lewis, T.L., Jr., Mao, T., Svoboda, K., and Arnold, D.B. (2009). Myosin-dependent targeting of transmembrane proteins to neuronal dendrites. Nat. Neurosci. *12*, 568–576.

Li, X., Gutierrez, D.V., Hanson, M.G., Han, J., Mark, M.D., Chiel, H., Hegemann, P., Landmesser, L.T., and Herlitze, S. (2005). Fast noninvasive activation and inhibition of neural and network activity by vertebrate rhodopsin and green algae channelrhodopsin. Proc. Natl. Acad. Sci. USA *102*, 17816–17821.

Lima, S.Q., Hromadka, T., Znamenskiy, P., and Zador, A.M. (2009). PINP: a new method of tagging neuronal populations for identification during in vivo electrophysiological recording. PLoS One *4*, e6099.

Lin, J.Y., Lin, M.Z., Steinbach, P., and Tsien, R.Y. (2009). Characterization of engineered channelrhodopsin variants with improved properties and kinetics. Biophys. J. *96*, 1803–1814.

Lozier, R.H., Bogomolni, R.A., and Stoeckenius, W. (1975). Bacteriorhodopsin: a light-driven proton pump in Halobacterium Halobium. Biophys. J. *15*, 955–962.

Marti, T., Otto, H., Mogi, T., Rösselet, S.J., Heyn, M.P., and Khorana, H.G. (1991). Bacteriorhodopsin mutants containing single substitutions of serine or threonine residues are all active in proton translocation. J. Biol. Chem. *266*, 6919–6927.

Maskos, U., Kissa, K., St Cloment, C., and Brûlet, P. (2002). Retrograde trans-synaptic transfer of green fluorescent protein allows the genetic mapping of neuronal circuits in transgenic mice. Proc. Natl. Acad. Sci. USA *99*, 10120–10125.

Nagel, G., Szellas, T., Huhn, W., Kateriya, S., Adeishvili, N., Berthold, P., Ollig, D., Hegemann, P., and Bamberg, E. (2003). Channelrhodopsin-2, a directly light-gated cation-selective membrane channel. Proc. Natl. Acad. Sci. USA *100*, 13940–13945.

Nathanson, J.L., Yanagawa, Y., Obata, K., and Callaway, E.M. (2009). Preferential labeling of inhibitory and excitatory cortical neurons by endogenous

tropism of adeno-associated virus and lentivirus vectors. Neuroscience *161*, 441–450.

Passini, M.A., Macauley, S.L., Huff, M.R., Taksir, T.V., Bu, J., Wu, I.H., Piepenhagen, P.A., Dodge, J.C., Shihabuddin, L.S., O'Riordan, C.R., et al. (2005). AAV vector-mediated correction of brain pathology in a mouse model of Niemann-Pick A disease. Mol. Ther. *11*, 754–762.

Paterna, J.C., Feldon, J., and Büeler, H. (2004). Transduction profiles of recombinant adeno-associated virus vectors derived from serotypes 2 and 5 in the nigrostriatal system of rats. J. Virol. *78*, 6808–6817.

Perreault, M.C., Bernier, A.P., Renaud, J.S., Roux, S., and Glover, J.C. (2006). C fragment of tetanus toxin hybrid proteins evaluated for muscle-specific transsynaptic mapping of spinal motor circuitry in the newborn mouse. Neuroscience *141*, 803–816.

Petreanu, L., Huber, D., Sobczyk, A., and Svoboda, K. (2007). Channelrhodopsin-2-assisted circuit mapping of long-range callosal projections. Nat. Neurosci. *10*, 663–668.

Petreanu, L., Mao, T., Sternson, S.M., and Svoboda, K. (2009). The subcellular organization of neocortical excitatory connections. Nature *457*, 1142–1145.

Ratzliff, A.H., Howard, A.L., Santhakumar, V., Osapay, I., and Soltesz, I. (2004). Rapid deletion of mossy cells does not result in a hyperexcitable dentate gyrus: implications for epileptogenesis. J. Neurosci. *24*, 2259–2269.

Ryan, M.D., and Drew, J. (1994). Foot-and-mouth disease virus 2A oligopeptide mediated cleavage of an artificial polyprotein. EMBO J. *13*, 928–933.

Sano, H., Nagai, Y., and Yokoi, M. (2007). Inducible expression of retrograde transynaptic genetic tracer in mice. Genesis *45*, 123–128.

Sato, M., Kubo, M., Aizawa, T., Kamo, N., Kikukawa, T., Nitta, K., and Demura, M. (2005). Role of putative anion-binding sites in cytoplasmic and extracellular channels of Natronomonas pharaonis halorhodopsin. Biochemistry *44*, 4775–4784.

Schröder-Lang, S., Schwärzel, M., Seifert, R., Strünker, T., Kateriya, S., Looser, J., Watanabe, M., Kaupp, U.B., Hegemann, P., and Nagel, G. (2007). Fast manipulation of cellular cAMP level by light in vivo. Nat. Methods *4*, 39–42.

Shu, X., Royant, A., Lin, M.Z., Aguilera, T.A., Lev-Ram, V., Steinbach, P.A., and Tsien, R.Y. (2009). Mammalian expression of infrared fluorescent proteins engineered from a bacterial phytochrome. Science *324*, 804–807.

Silberberg, G., Wu, C., and Markram, H. (2004). Synaptic dynamics control the timing of neuronal excitation in the activated neocortical microcircuit. J. Physiol. *556*, 19–27.

Simon, S.M., and Blobel, G. (1993). Mechanisms of translocation of proteins across membranes. Subcell. Biochem. *21*, 1–15.

Sineshchekov, O.A., Govorunova, E.G., Jung, K.H., Zauner, S., Maier, U.G., and Spudich, J.L. (2005). Rhodopsin-mediated photoreception in cryptophyte flagellates. Biophys. J. *89*, 4310–4319.

Sohal, V.S., Zhang, F., Yizhar, O., and Deisseroth, K. (2009). Parvalbumin neurons and gamma rhythms enhance cortical circuit performance. Nature *459*, 698–702.

Stoeckenius, W., and Bogomolni, R.A. (1982). Bacteriorhodopsin and related pigments of halobacteria. Annu. Rev. Biochem. *51*, 587–616.

Sugita, M., and Shiba, Y. (2005). Genetic tracing shows segregation of taste neuronal circuitries for bitter and sweet. Science *309*, 781–785.

Tang, W., Ehrlich, I., Wolff, S.B., Michalski, A.M., Wölfl, S., Hasan, M.T., Lüthi, A., and Sprengel, R. (2009). Faithful expression of multiple proteins via 2A-peptide self-processing: a versatile and reliable method for manipulating brain circuits. J. Neurosci. *29*, 8621–8629.

Tengholm, A., and Gylfe, E. (2009). Oscillatory control of insulin secretion. Mol. Cell. Endocrinol. *297*, 58–72.

Tønnesen, J., Sørensen, A.T., Deisseroth, K., Lundberg, C., and Kokaia, M. (2009). Optogenetic control of epileptiform activity. Proc. Natl. Acad. Sci. USA *106*, 12162–12167.

Tsai, H.C., Zhang, F., Adamantidis, A., Stuber, G.D., Bonci, A., de Lecea, L., and Deisseroth, K. (2009). Phasic firing in dopaminergic neurons is sufficient for behavioral conditioning. Science *324*, 1080–1084.

Tsunoda, S.P., Ewers, D., Gazzarrini, S., Moroni, A., Gradmann, D., and Hegemann, P. (2006). H+ -pumping rhodopsin from the marine alga Acetabularia. Biophys. J. *91*, 1471–1479.

Wang, H., Peca, J., Matsuzaki, M., Matsuzaki, K., Noguchi, J., Qiu, L., Wang, D., Zhang, F., Boyden, E., Deisseroth, K., et al. (2007). High-speed mapping of synaptic connectivity using photostimulation in Channelrhodopsin-2 transgenic mice. Proc. Natl. Acad. Sci. USA *104*, 8143–8148.

Wu, Y.I., Frey, D., Lungu, O.I., Jaehrig, A., Schlichting, I., Kuhlman, B., and Hahn, K.M. (2009). A genetically encoded photoactivatable Rac controls the motility of living cells. Nature *461*, 104–108.

Yooseph, S., Sutton, G., Rusch, D.B., Halpern, A.L., Williamson, S.J., Remington, K., Eisen, J.A., Heidelberg, K.B., Manning, G., Li, W., et al. (2007). The Sorcerer II Global Ocean Sampling expedition: expanding the universe of protein families. PLoS Biol. *5*, e16.

Yoshimura, Y., Dantzker, J.L., and Callaway, E.M. (2005). Excitatory cortical neurons form fine-scale functional networks. Nature *433*, 868–873.

Zhang, Y.P., and Oertner, T.G. (2007). Optical induction of synaptic plasticity using a light-sensitive channel. Nat. Methods *4*, 139–141.

Zhang, F., Wang, L.P., Boyden, E.S., and Deisseroth, K. (2006). Channelrhodopsin-2 and optical control of excitable cells. Nat. Methods *3*, 785–792.

Zhang, F., Wang, L.P., Brauner, M., Liewald, J.F., Kay, K., Watzke, N., Wood, P.G., Bamberg, E., Nagel, G., Gottschalk, A., and Deisseroth, K. (2007a). Multimodal fast optical interrogation of neural circuitry. Nature *446*, 633–639.

Zhang, F., Aravanis, A.M., Adamantidis, A., de Lecea, L., and Deisseroth, K. (2007b). Circuit-breakers: optical technologies for probing neural signals and systems. Nat. Rev. Neurosci. *8*, 577–581.

Zhang, F., Prigge, M., Beyrière, F., Tsunoda, S.P., Mattis, J., Yizhar, O., Hegemann, P., and Deisseroth, K. (2008). Red-shifted optogenetic excitation: a tool for fast neural control derived from Volvox carteri. Nat. Neurosci. *11*, 631–633.

Zhang, F., Gradinaru, V., Adamantidis, A.R., Durand, R., Airan, R.D., de Lecea, L., and Deisseroth, K. (2010). Optogenetic interrogation of neural circuits: technology for probing mammalian brain structures. Nat. Protoc. *5*, 439–456.

Zhao, S., Cunha, C., Zhang, F., Liu, Q., Gloss, B., Deisseroth, K., Augustine, G.J., and Feng, G. (2008). Improved expression of halorhodopsin for light-induced silencing of neuronal activity. Brain Cell Biol. *36*, 141–154.

EXTENDED EXPERIMENTAL PROCEDURES

Opsin Sources

All opsins described here have been optimized for mammalian expression by changing each gene's codon usage to conform to human codon usage distribution (http://www.kazusa.or.jp/codon/cgi-bin/showcodon.cgi?species=9606). The GenBank accession code for the original AR, BR, and GtR3 sequences are DQ074124, M11720, and EG722553.

DNA Constructs

All NpHR variants were produced by PCR amplification of the NpHR-EYFP construct previously published (Zhang et al., 2007b) and cloned in-frame into the AgeI and EcoRI restriction sites of a lentivirus carrying the CaMKIIα or Synapsin-1 promoters according to standard molecular biology protocols. A similar strategy was used for BR and AR. GtR3 was identified through genomic searches. All opsins described here have been optimized for mammalian expression by changing each gene's codon usage to conform to human codon usage distribution (http://www.kazusa.or.jp/codon/cgi-bin/showcodon.cgi?species=9606), and the optimized sequence was custom synthesized (DNA2.0, Inc., Menlo Park, CA). The GenBank accession codes for the original AR, BR, and GtR3 sequences are DQ074124, M11720, and EG722553. pAAV-EF1a-mCherry-IRES-WGA-Cre vector was constructed using standard molecular biology protocols. Codons for the WGA and Cre genes were optimized for expression in mammalian cells. The genes were synthesized by DNA2.0 (Menlo Park, CA). Cre was fused in-frame to the C-term of WGA, which in turn was fused to IRES. The mCherry-IRES-WGA-Cre bicistronic expression cassette was designed using the EMCV IRES sequence. The pAAV-EF1a plasmid backbone is the same as described previously (Sohal et al., 2009; Tsai et al., 2009). pAAV-hSyn-eNpHR3.0-EFYP-P2A-ChR2H134R-mCherry was constructed with a 120-mer primer (5′caagttctgctacgagaacgaggtgggctccggagccacgaacttctctctgttaaagcaagcagg agacgtggaagaaaaccccggtcccatggactatggcggcgctttgtctgccg 3′) that contained the p2A region with the ER export sequence at the 5′ end and 20 bases of the start of hChR2 at the 3′ end. First, the ChR2(H134R)-mCherry fragment was amplified using the 120-mer as the forward primer and 5′–atatcgaattctcattacttgtacagctcgt– 3′ as the reverse primer. Second, this amplified product was used as a reverse primer along with the forward primer 5′–ccggatccccgggtaccggtaggccaccatgacagagaccctgcct– 3′ to fuse eNpHR 3.0-EYFP to ChR2 (H134R)-mCherry with the p2A region interposed. The 3.4 Kb fragment was then purified and cloned into the BamHI and EcoRI sites of the pAAV-hSyn vector. All constructs were fully sequenced for accuracy of cloning; updated maps are available online at http://www.optogenetics.org.

Lentivirus Preparation and Titering

Lentiviruses for cultured neuron infection and for in vivo injection were produced as previously described (Zhang et al., 2007b). Viral titering was performed in HEK293 cells that were grown in 24-well plates and inoculated with 5-fold serial dilutions in the presence of polybrene (8 μg/ml). After 4 days, cultures were resuspended in PBS and sorted for EYFP fluorescence on a FACScan flow cytometer (collecting 20,000 events per sample) followed by analysis using FlowJo software (Ashland, OR). The titer of the virus was determined as follows: [(% of infected cells) × (total number of cells in well) × (dilution factor)]/ (volume of inoculum added to cells) = infectious units/ml. The titer of viruses for culture infection was 10^5 i.u. /ml. The titer of concentrated virus for in vivo injection was 10^{10} i.u. /ml.

Hippocampal Cultures

Primary cultured hippocampal neurons were prepared from P0 Sprague-Dawley rat pups. The CA1 and CA3 regions were isolated, digested with 0.4 mg/mL papain (Worthington, Lakewood, NJ), and plated onto glass coverslips precoated with 1:30 Matrigel (Becton Dickinson Labware, Bedford, MA) at a density of 65,000/cm^2. Cultures were maintained in a 5% CO_2 humid incubator with Neurobasal-A medium (Invitrogen Carlsbad, CA) containing 1.25% FBS (Hyclone, Logan, UT), 4% B-27 supplement (GIBCO, Grand Island, NY), 2 mM Glutamax (GIBCO), and FUDR (2 mg/ml, Sigma, St. Louis, MO).

Calcium Phosphate Transfection

6-10 *div* hippocampal neurons were grown at 65,000 cells/well in a 24-well plate. DNA/$CaCl_2$ mix for each well: 1.5-3 μg DNA (-QIAGEN endotoxin-free preparation) + 1.875 μl 2M $CaCl_2$ (final Ca^{2+} concentration 250 mM) in 15 μl total H_20. To DNA/$CaCl_2$ was added 15 μl of 2X HEPES-buffered saline (pH 7.05), and the final volume was mixed well by pipetting. After 20 min at RT, the 30 μl DNA/$CaCl2_2$/HBS mixture was dropped into each well (from which the growth medium had been temporarily removed and replaced with 400 μl warm MEM) and transfection allowed to proceed at 37C for 45-60 min. Each well was then washed with 3 X 1mL warm MEM and the growth medium replaced. Opsin expression was generally observed within 20-24 hr.

Electrophysiology

Hippocampal cultures grown on coverslips were transduced at 4 div with titer-matched viruses for all constructs (final dilution 10^4 i.u. /ml in neuronal growth medium) and allowed to express for one week. Whole-cell patch clamp recordings were performed as previously described (intracellular solution: 129 mM K-gluconate, 10 mM HEPES, 10 mM KCl, 4 mM MgATP, 0.3 mM Na_3GTP, titrated to pH 7.2; extracellular Tyrode: 125 mM NaCl, 2 mM KCl, 3 mM $CaCl_2$, 1 mM $MgCl_2$, 30 mM glucose, and 25 mM HEPES, titrated to pH 7.3). For voltage clamp recordings cells were held at −70mV. Light in the visible range was delivered from a 300W DG-4 lamp (Sutter Instruments, Novato, CA) through filters of different wavelength selectivity (Semrock, Rochester, NY) and a Leica 40X/0.8NA water

objective. Filters, except for power spectra, (given here as wavelength in nm / bandwidth in nm / output power in mW/mm^2) were: 406 / 15 / 3; 472 / 30 / 18.5; 560 / 14 / 7; 589 / 15 / 7.5; 593 / 40 / 15.5; 630 / 20 / 3.5. Far-red and near-infrared light delivery: light (7 mW/mm^2) for 660nm inhibition was delivered using a light emitting diode and a 40x/.8 NA water objective. Light (7mW/mm^2) for 680nm inhibition was delivered using the X-Cite 120W halogen light source through a 680 ± 13nm filter and a 40x/0.8 NA water objective. Light delivery for eNPAC, ChR2(H134R), and eNpHR3.0 power spectra was delivered from a 300W DG-4 lamp fitted with a Lambda 10-3 filter wheel (Sutter Instruments) with a 10-position wheel for 25-mm filters of different wavelengths and a 40X/0.8NA water objective. Filters (given here as wavelength in nm / bandwidth in nm / output power in mW/mm^2) were: 387 / 10 / 3.5; 406 / 15 / 3.5; 427 / 10 / 4.0; 445 / 20 / 4.0; 470 / 22 / 4.0; 494 / 20 / 4.5; 520 / 15 / 4.5; 542 / 27 / 5.0; 560 / 20 / 5.0; 590 / 20 / 3.5; 630 / 20 / 3.5. For Figures 1, 3A–3D, and 4 and Figure S2, confocal images and whole-cell patch clamp data are from cultured hippocampal neurons either transfected (confocal data) or transduced (patch data) with lentiviral NpHR, BR, GtR3 and AR-based constructs, and allowed to express for one week. Expression was driven by the human Synapsin I promoter and visualized by fusion to EYFP.

Immunohistochemistry

Primary hippocampal cultures were infected at 4 div with titer matched virus (final dilution 10^4 i.u./ml in neuronal growth medium). At 14 div cultures were fixed for 30 min with ice-cold 4% paraformaldehyde and then permeabilized for 30 min with 0.4% saponin in 2% normal donkey serum (NDS). Primary antibody incubations were performed overnight at 4°C using a monoclonal marker of endoplasmic reticulum recognizing endogenous ER-resident proteins containing the KDEL retention signal (KDEL 1:200, Abcam, Cambridge, MA). Cy3-conjugated secondary antibodies (Jackson Laboratories, West Grove, PA) were applied in 2% NDS for 1 hr at room temperature. Images were obtained on a Leica confocal microscope using a 63X/1.4NA oil objective.

Stereotactic Injection into the Rodent Brain

Adult mice and Long-Evans rats were housed according to the approved protocols at Stanford. All surgeries were performed under aseptic conditions. The animals were anesthetized with intraperitoneal injections of a ketamine (80 mg/kg)/xylazine (15-20 mg/kg) cocktail (Sigma). The head was placed in a stereotactic apparatus (Kopf Instruments, Tujunga, CA; Olympus stereomicroscope). Ophthalmic ointment was applied to prevent eye drying. A midline scalp incision was made and a small craniotomy was performed using a drill mounted on the stereotactic apparatus (Fine Science Tools, Foster City, CA). The virus was delivered using a 10 μl syringe and a thin 34 gauge metal needle; the injection volume and flow rate (1 μl at 0.1 μl/min) was controlled with an injection pump from World Precision Instruments (Sarasota, FL). After injection the needle was left in place for 5 additional minutes and then slowly withdrawn. The skin was glued back with Vetbond tissue adhesive. The animal was kept on a heating pad until it recovered from anesthesia. Buprenorphine (0.03 mg/kg) was given subcutaneously following the surgical procedure to minimize discomfort. For the experiment in Figure 2A, to cover a large area in dorsal CA1, 1μl of concentrated lentivirus (10^{10} i.u. /ml) carrying eNpHR3.1 (a shorter form of eNpHR3.0 with the N-terminal signal peptide, the first 17 amino acids of original NpHR, removed) under the CaMKIIα promoter was microinjected into 2 sites in each hippocampus (site one: anteroposterior −1.5 mm from bregma; lateral, ± 1 mm; ventral, 1.5 mm; site two: AP, −2.5 mm from bregma; lateral, ± 2 mm; ventral, 1.5 mm). For Figures 2D and 2E, two different adeno-associated viruses (AAVs) (virus titer 2x10^{12} g.c./mL), were stereotactically injected during the same surgery with an injection speed of 0.15ul/min. High-titer (2x10^{12} g.c./mL) AAV was produced by the UNC VectorCore. For Figure 2D, double-floxed cre-dependent AAV5 carrying eNpHR3.0–EYFP (AAV5-Ef1a-DIO-eNpHR3.0-EYFP) was injected into M1, and AAV2-Ef1α-mCherry-IRES-WGA-Cre was injected into S1 of adult Long-Evans rats. 1 μl of virus was delivered at five different sites defined by the following coordinates: M1 injection I: AP, +1 mm from bregma; lateral, 1.5 mm; ventral, 2 mm; M1 injection II: AP, +2 mm; lateral, 1.5 mm; ventral, 2 mm; S1 injection I: AP, −0.3 mm; lateral, 3.4 mm; ventral, 2 mm; S1 injection II: AP, −1.3 mm; lateral, 3 mm; ventral, 2 mm; S1 injection III: AP, −2.12 mm; lateral, 3 mm; ventral, 2 mm. For Figure 2E, 1 μl of virus was injected bilaterally into the dentate gyrus (DG) of adult BL6 mice. AAV8-EF1a-DIO-ChR2-EYFP was injected in the right DG and of AAV2-EF1a-mCherry-IRES-WGA-Cre was injected in the left DG with the following coordinates: AP, −2.1 mm from bregma; lateral, ± 1.05 mm; ventral, 2.1 mm.

In Vivo Optrode Recordings

To validate opsin functionality in the WGA-Cre system simultaneous optical stimulation and electrical recording in living rodents was conducted as described previously (Gradinaru et al., 2007) using an optrode composed of an extracellular tungsten electrode (1 MΩ, ~125 μm) attached to an optical fiber (~200 μm) with the tip of the electrode deeper (~0.4 mm) than the tip of the fiber to ensure illumination of the recorded neurons. The optical fiber was coupled to a 473 nm (for ChR2) or 560 nm (for eNpHR3.0) laser diode (10 mW fiber output) from CrystaLaser. Optrode recordings were conducted in rodents anesthetized with 1.5% isoflurane and the optode was placed through small craniotomies created above target regions. pClamp 10 and a Digidata 1322A board were used to both collect data and generate light pulses through the fiber. The recorded signal was band pass filtered at 300Hz low/5 kHz high (1800 Microelectrode AC Amplifier). For precise placement of the fiber/electrode pair, stereotactic instrumentation was used.

Tissue Slice Preparation

For preparation of brain slices, mice or rats were sacrificed 4 to 5 weeks after viral injection. Rodents were perfused with 20ml of ice-cold PBS, followed by 20 ml of 4% paraformaldehyde. The brains were then fixed overnight in 4% paraformaldehyde, and transferred to 30% sucrose solution for 2 days. Brains were frozen and coronal slices (40 μm) were prepared using a Leica SM2000R cryostat,

and preserved in 4°C in cryoprotectant (25% glycerol, 30% ethylene glycol, in PBS). Slices (DAPI stain 1:50,000) were mounted with PVA-DABCO on microscope slides, and single confocal optical sections (e.g., through dorsal CA1 region, ~1-2.5mm posterior to bregma or the dorsal subiculum, 2.7-3 mm posterior to bregma) were acquired using a 10X air and 40X/1.4NA oil objectives on a Leica confocal microscope.

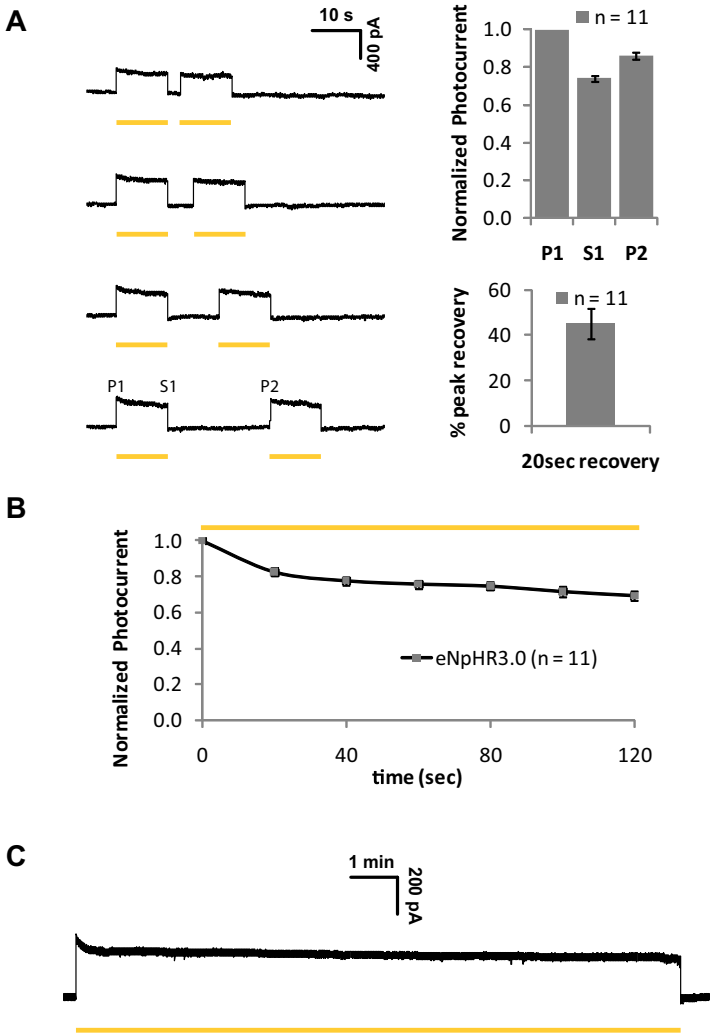

Figure S1. Stable and potent photocurrents for eNpHR3.0 over both short and long timescales relevant to physiology and behavior, Related to Figure 1

(A) Stability and recovery over seconds: representative traces (*left*) showing photocurrents in cells expressing eNpHR3.0 when exposed to pairs of 10 s long yellow light pulses separated in time by (top to bottom): 2.5 s, 5 s, 10 s, 20 s. Summary plot for pulses 20 s apart showing normalized average photocurrent levels (*top right*) in cells expressing eNpHR3.0 (P1 = first pulse peak, 1.00; S1 = first pulse steady state, 0.74 ± 0.01; P2 = second pulse peak, 0.86 ± 0.02; *n* = 11 cells). Summary plot for pulses 20 s apart showing ~50% peak recovery, (P2-S1)/(P1-S1), (*bottom right*); after 20 s, the peak recovers to (45.2 ± 6.6) %.

(B) Stability over minutes: timecourse of eNpHR3.0 normalized photocurrents for long-term continuous light exposure (*n* = 11 cells). Values plotted are mean ± s.e.m for all above.

(C) Stability over >10 min: outward current of eNpHR3.0. Note the stability of the steady state. Light delivery (593nm) for all above is indicated by the yellow bar. Output power density: 2.5mW/mm^2.

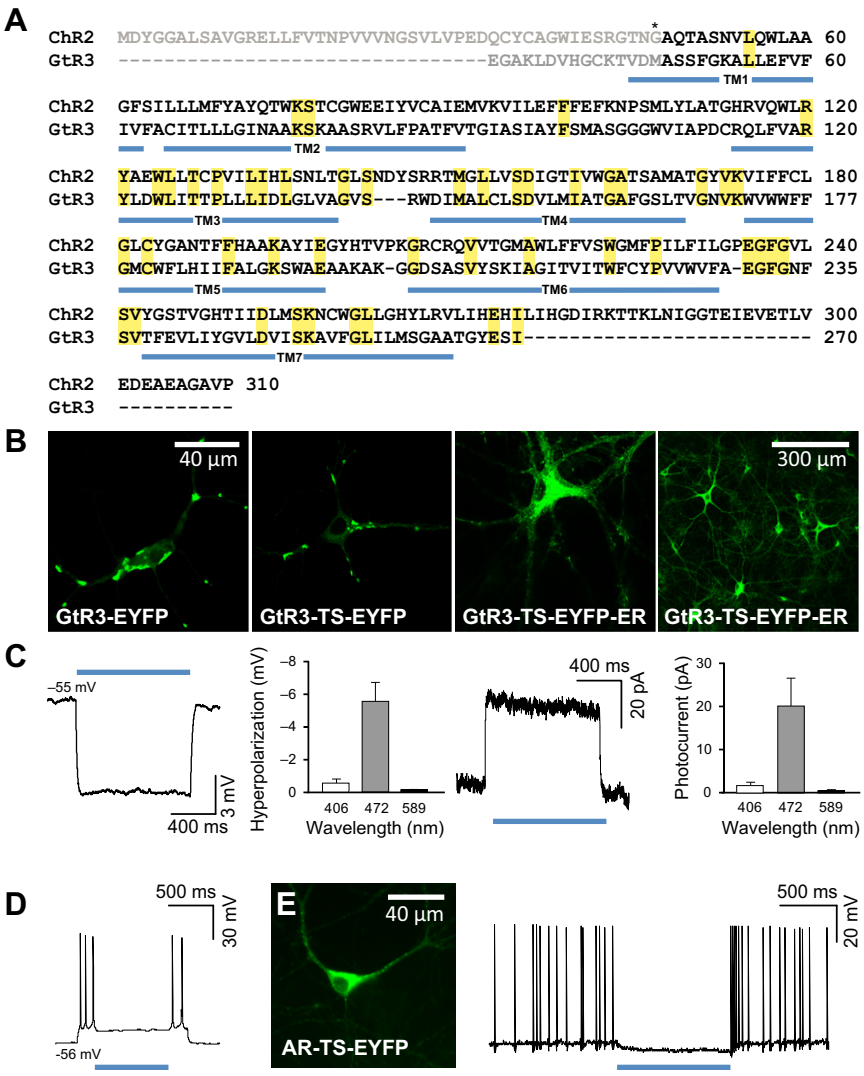

Figure S2. Additional Trafficking-Enhanced Tools for Blue Inhibition, Related to Figure 4

(A) New opsin sequence: *G. theta* rhodopsin-3 or GtR3. The EST sequence included all seven transmembrane helices; the 5′ amino acid sequence was provided from ChR2 (transmembrane motifs: blue bars; conserved residues: yellow; truncation site for signal peptide: *; signal peptide provided from ChR2: gray).

(B) Confocal images of hippocampal neurons; note GtR3 formed aggregates as with unmodified NpHR or BR (*left*). Provision of the TS motif before EYFP decreased the size of the aggregates but did not abolish them (*middle*). Only when the ER export motif (FCYENEV) was also provided to the C terminus were aggregates abolished (*right*).

(C) Sample current clamp (*left*) and voltage clamp (*right*) traces and summary data show GtR3 function under 472nm light (18.5 mW/mm^2). Light induced outward photocurrent summary (*left bar graph)* and corresponding hyperpolarization summary (*right bar graph*) for blue light peak. Corresponding photocurrents and hyperpolarization were: 0.5 ± 0.4 pA and 0.12 ± 0.09 mV for yellow light (589nm; 7.5 mW/mm^2); 20.0 ± 6.7 pA and 5.6 ± 1.2 mV for blue light (472nm; 18.5 mW/mm^2); 1.7 ± 0.9 pA and 0.6 ± 0.3 mV for purple light (406nm; 3 mW/mm^2). Mean ± s.e.m plotted; n = 10; input resistance was similar for all neurons (113.5 ± 24.2 MΩ).

(D) Illumination with blue light (472nm; 18.5 mW/mm^2) sufficed to inhibit spiking induced by current injection in GtR3-expressing neurons.

(E) TS-modification enhanced AR function (as AR showed no aggregates the ER export signal was not used). Illumination with blue light (472nm; 18.5 mW/mm^2) sufficed to inhibit spiking. Additional molecular engineering is required to establish utility of these two opsin genes which cannot outperform eNpHR3.0.